

Diffraction Anomalous Fine Structure: A New X-Ray Structural Technique

H. Stragier, J. O. Cross, J. J. Rehr, and Larry B. Sorensen

Department of Physics, FM-15, University of Washington, Seattle, Washington 98195

C. E. Bouldin and J. C. Woicik

National Institute of Standards and Technology, Gaithersburg, Maryland 20899

(Received 3 April 1992)

A new x-ray structural technique, diffraction anomalous fine structure (DAFS), which combines the long-range order sensitivity of diffraction techniques with the short-range order sensitivity of absorption techniques, is described. We demonstrate that synchrotron DAFS measurements for the Cu(111) and Cu(222) Bragg reflections provide the same local atomic structural information as x-ray absorption fine structure and describe how DAFS can be used to provide enhanced site and spatial sensitivities for polyatomic and/or spatially modulated structures.

PACS numbers: 61.10.-i, 07.85.+n, 78.70.Ck, 78.70.Dm

In 1927, Dirac derived the nonrelativistic, quantum electrodynamic photon-atom scattering cross section and the corresponding forward dispersion relation between the real, f_1 , and imaginary, f_2 , components of the anomalous scattering amplitude, Δf [1]. The generalization to nonzero momentum transfer implies that, in principle, absorptionlike information can be obtained from scattering measurements [2]. In this Letter, we demonstrate that this is true in practice: The short-range local atomic order information traditionally obtained from x-ray absorption measurements can also be obtained easily and accurately from energy-dependent x-ray diffraction intensity measurements at fixed momentum transfer. The reason that diffraction can be used to provide absorptionlike information is because f_1 and f_2 are related by causality and Δf is almost independent of the momentum transfer.

The two principal x-ray techniques currently used to obtain atomic structural information are x-ray diffraction and x-ray absorption. Traditional x-ray diffraction measurements provide information about the ordered, long-range atomic structure: the spatial persistence and fluctuations of the unit cells via high-resolution diffraction, and the average, long-range, unit cell internal structure via crystallography. X-ray absorption fine-structure (XAFS) measurements provide local structural information: the near-neighbor bond lengths, types, and disorders around the specifically excited absorbing atoms. Here, we demonstrate that precise energy-dependent x-ray diffraction anomalous fine-structure (DAFS) measurements for the (111) and (222) Bragg reflections of Cu metal contain the same local atomic structural information as XAFS measurements.

Although there were numerous early observations of DAFS [3], it is surprising that there were not any attempts to use the DAFS oscillations to provide the analog of XAFS short-range information until quite recently [4], and that there have apparently been no attempts to use the enhanced simultaneous diffractionlike and absorptionlike sensitivities available from DAFS measurements. Since DAFS combines all of the capabilities of diffraction

and XAFS into a single technique, it provides advantages that neither technique possesses separately: (1) DAFS provides short-range order information about the set or subset of long-range ordered atoms selected by the diffraction condition. (2) DAFS is chemically and valence specific, and is sensitive to the positions of neighboring atoms even when the neighbors have low atomic numbers. (3) The relative contributions of chemically identical, but site inequivalent, atoms can be separated by measuring the DAFS intensities of Bragg peaks with different diffraction structure factor contributions.

In nonrelativistic quantum mechanics, neglecting the magnetic scattering terms, the atomic scattering amplitude, $f = f_0 + \Delta f$, is the sum of the nonresonant Thomson scattering amplitude, $f_0(\mathbf{Q})$, and the resonant anomalous scattering amplitude, $\Delta f(\mathbf{k}_1, \mathbf{k}_2, E)$, which is proportional to [5,6]

$$\sum_j \sum_n \frac{\langle j | \hat{\mathbf{e}}_2 \cdot \mathbf{p} e^{-i\mathbf{k}_2 \cdot \mathbf{r}} | n \rangle \langle n | \hat{\mathbf{e}}_1 \cdot \mathbf{p} e^{+i\mathbf{k}_1 \cdot \mathbf{r}} | j \rangle}{E_n - E_j - \hbar\omega - i\alpha} + \frac{\langle j | \hat{\mathbf{e}}_1 \cdot \mathbf{p} e^{+i\mathbf{k}_1 \cdot \mathbf{r}} | n \rangle \langle n | \hat{\mathbf{e}}_2 \cdot \mathbf{p} e^{-i\mathbf{k}_2 \cdot \mathbf{r}} | j \rangle}{E_n - E_j + \hbar\omega - i\alpha}. \quad (1)$$

The Thomson amplitude depends only on the momentum transfer $\hbar\mathbf{Q} = \hbar(\mathbf{k}_2 - \mathbf{k}_1)$, and is proportional to the Fourier transform of the atomic charge distribution. In contrast, $\Delta f(\mathbf{k}_1, \mathbf{k}_2, E)$ depends separately on the incident and scattered photon wave vectors \mathbf{k}_1 and \mathbf{k}_2 and on the photon energy E . In general, Δf is a tensor, and is not proportional to the Fourier transform of the total or subshell charge density [7]. However, it has been established experimentally that the \mathbf{k}_1 and \mathbf{k}_2 dependencies are often very small, and consequently the full photon energy- and momenta-dependent $\Delta f(\mathbf{k}_1, \mathbf{k}_2, E)$ is conventionally [6] approximated by its forward scattering limit, denoted $\Delta f(E) = f_1(E) + if_2(E)$. The experimental results in this paper confirm the validity of this approximation to the level of our measurements (2-5)% for both the Cu(111) and Cu(222) Bragg reflections.

The atomic scattering amplitude for condensed phase

atoms can be further subdivided into smooth and oscillating contributions. The smooth, bare atom contribution, $f_0(\mathbf{Q}) + f_1^0(E) + if_2^0(E)$, is the same as that for isolated single atom x-ray scattering. The oscillating DAFS contribution, $f_2^0(E)\chi(E)$ with $\chi = \chi_1 + i\chi_2$, is produced by the neighboring atoms and provides local structural information for condensed phase atoms. This separation of $f = [f_0(Q) + f_1^0(E) + if_2^0(E)] + [f_2^0(E)\chi(E)]$ into atomic and fine-structure components is analogous to the usual XAFS separation.

When the \mathbf{k}_1 and \mathbf{k}_2 dependence of Δf can be neglected, the DAFS $\chi(E)$, in the single-scattering dipole approximation, is proportional to [8]

$$-\sum_j N_j \frac{t_j(2k)}{R_j^2} \exp(-2k^2\sigma_j^2) \times \exp(-2R_j/\Lambda_j) \exp[-i(2kR_j + \delta_j(k))]. \quad (2)$$

Here the photoelectron wave number k is related to the incident photon energy E and the binding energy E_0 by $k = [2m(E - E_0)/\hbar^2]^{1/2}$; the sum is over neighboring atomic shells, labeled by j ; and the parameters are the coordination numbers N_j , the photoelectron backscattering amplitudes $t_j(k)$, the bond-length disorders σ_j , the mean free path and lifetime factors Λ_j , the neighbor separations R_j , and the photoelectron phase shifts $\delta_j(k)$. The DAFS χ is the complex generalization of the standard XAFS χ_a , which has been extensively studied experimentally and theoretically [9]. They are related by $\chi_a(E) = \text{Im}\chi(\mathbf{k}_1 = \mathbf{k}_2, E)$. Consequently the DAFS χ oscillations have the form $-\cos[2kR_j + \delta_j(k)] + i\sin[2kR_j + \delta_j(k)]$, while the XAFS χ_a oscillations have the form $\sin[2kR_j + \delta_j(k)]$.

For kinematically scattering monatomic systems, the measured DAFS intensity, $I(\mathbf{Q}, E) \sim |f(\mathbf{Q}, E)|^2 A(\mathbf{Q}, E)$, is proportional to the square of the atomic scattering amplitude, $f(\mathbf{Q}, E)$, times an x-ray absorption correction, $A(\mathbf{Q}, E)$. The absorption correction, $A(\mathbf{Q}, E) = [1 - \exp(-2\mu t/\sin\theta)]/2\mu$, also produces $\chi_2(E)$ fine structure in the DAFS intensity due to the XAFS modulation of the x-ray absorption coefficient, $\mu(E) = \mu_0[1 + \chi_2(E)]$. For a thin sample, the absorption correction can be approximated by $A(\mathbf{Q}, E) \sim d(1 - \mu d)$, with $d = t/\sin\theta$. The diffraction contributions to the DAFS oscillations come from the $(\chi_1 + i\chi_2)$ contributions to the square of the atomic scattering amplitude, $|f|^2 = (f_0 + f_1^0 + f_2^0\chi_1)^2 + (f_2^0\chi_2)^2$. Expanding $|f|^2$ and discarding small higher-order terms yields $|f|^2 \sim [(f_0 + f_1^0)^2 + (f_2^0)^2] + [2(f_0 + f_1^0)f_2^0\chi_1 + [2(f_2^0)^2]\chi_2]$. Consequently, χ_1 and χ_2 appear linearly in the DAFS intensities.

The data were collected at beam line X23A2, at the National Synchrotron Light Source. The incident energy was selected with a Si(220) double-crystal monochromator which provided an energy spread of about 2 eV FWHM and a flux of 5×10^9 photons per second in a 1-mm-high by 5-mm-wide beam. A vertical scattering plane was chosen so that no scattering polarization cor-

rection was required. No DAFS polarization correction was required because of the high symmetry of the Cu lattice. The diffracted beam was analyzed with a 3-mm-high by 5-mm-wide slit located 27 cm from the sample; this provided adequate suppression of the fluorescence from the sample while accepting essentially all of the diffracted beam. At each energy, the diffractometer was adjusted to keep the momentum transfer fixed; to obtain reliable intensity measurements it was essential to accurately track the Bragg peak versus energy. The sample was a 25-mm-diam 2000-Å-thick Cu(111) film grown epitaxially on mica. The c -axis mosaic spread of the film was $\sim 0.25^\circ$ FWHM. A thin sample was chosen to minimize the absorption correction. The diffracted intensities were 3×10^7 photons/sec for the Cu(111) Bragg reflection and 1×10^7 photons/sec for the Cu(222) reflection. Since the statistical noise limit for DAFS measurements is set by Poisson statistics, we used integral, current mode techniques to maximize the number of detected photons; both the incident and diffracted intensities were measured with nitrogen-filled ionization chambers. To reduce the effects of synchrotron and monochromator noise, the diffraction intensity at each energy was corrected for incident intensity variations. The fluorescence XAFS from the Cu film was measured simultaneously with the DAFS signals.

The measured Cu(111) and Cu(222) diffraction intensities and the fluorescence XAFS intensity are shown in Fig. 1. The cusp in the Bragg intensity is produced by the interference between the real part of the anomalous

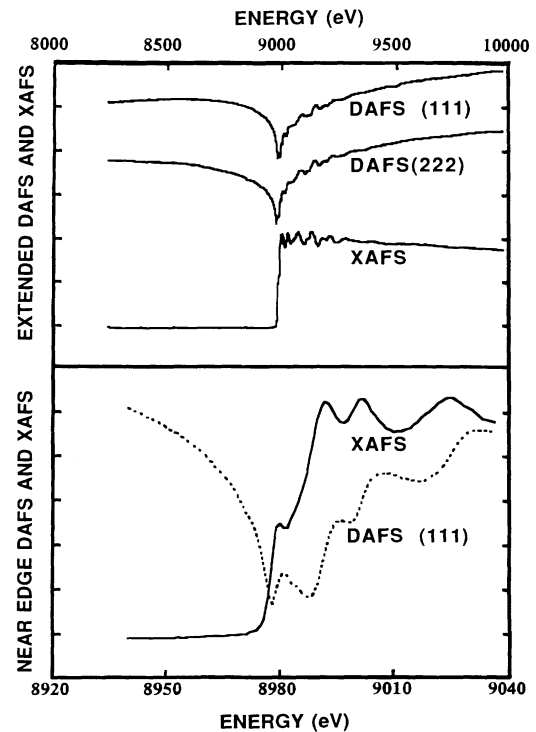


FIG. 1. Comparison of the raw DAFS and XAFS signals. The normalized oscillations are about 12% peak to peak.

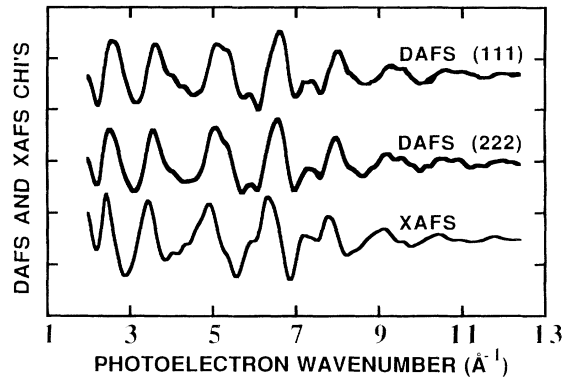


FIG. 2. The background-subtracted and normalized DAFS and XAFS signals. Two DAFS data sets have been overlapped to show the reproducibility of the measurements.

amplitude, f_1 , and the Thompson amplitude, f_0 ; it drops at the edge energy, $E_0 = 8979$ eV, to about 50% of the preedge intensity at 8500 eV for the Cu(111) reflection and to about 25% for the Cu(222) reflection. This difference in the relative cusp drop between the two reflections is caused by the decrease in f_0 with Q . The fine-structure oscillations above the absorption edge are present in both the DAFS and XAFS signals and have similar sizes, 12% peak to peak, when normalized to their corresponding cusp drop or edge step sizes.

Figure 2 shows the corresponding fine-structure signals calculated by subtracting a smooth fitted spline from the data in Fig. 1 and then normalizing. The strong similarity between the Cu(111) and the Cu(222) DAFS signals is evident, as is an apparent difference between the two DAFS signals and the XAFS signal. Figure 3 shows the Fourier-transform magnitudes of the three signals in Fig. 2. The agreement between the two DAFS and the XAFS Fourier transforms is very good. Consequently, although the multishell DAFS and XAFS signals in Fig. 2 appear to be different, they actually have identical Fourier magnitudes and therefore can only differ in their phases. Figure 4 shows that the DAFS signals for each shell have the same phase shift for a fixed Bragg reflection, but the (111) and (222) reflections have different phase shifts. The different appearances of the signals in Fig. 2 are produced by these phase shifts.

The DAFS-to-XAFS phase shifts determined using multiple back-filtered data sets, assuming that the XAFS and DAFS bond lengths are identical, are Cu(111) first shell $90^\circ \pm 6^\circ$ and second shell $83^\circ \pm 12^\circ$; and Cu(222) first shell $70^\circ \pm 6^\circ$ and second shell $64^\circ \pm 12^\circ$. For the (111) reflection, the χ_2 DAFS contribution and the χ_2 absorption correction contribution accidentally canceled, leaving only the $2(f_0 + f_1^0)f_2^0\chi_1$ oscillating DAFS cosine contribution. Consequently, the Cu(111) first and second shells are shifted by $\sim 90^\circ$ with respect to the Cu XAFS signal. For the (222) reflection, the DAFS χ_2 component is larger than the absorption χ_2 contribution and the

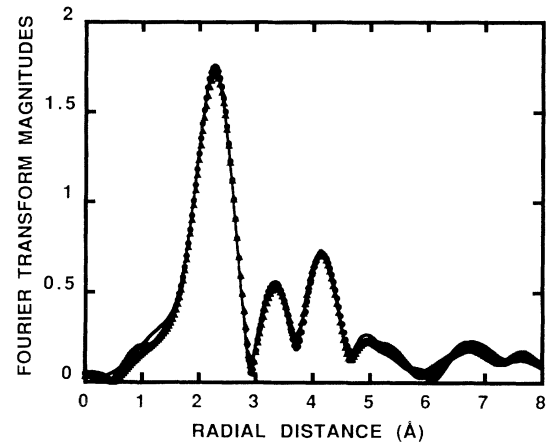


FIG. 3. The Fourier transform magnitudes of the DAFS and XAFS signals. The symbols are as follows: circles, Cu(111) DAFS; triangles, Cu(222) DAFS; and lines, Cu XAFS. The transforms are nearly identical, demonstrating that DAFS and XAFS contain the same local atomic structural information.

Cu(222) DAFS signals are shifted by $\sim 67^\circ$. These measured phase shifts agree very well with the values calculated from the sample thickness t , and tabulated values of f_0 , f_1 , f_2 , and μ [8].

Without constraining the distances to be equal, and us-

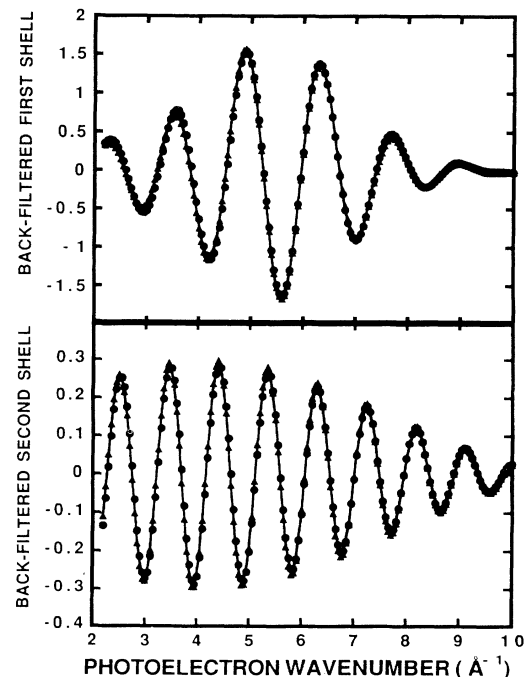


FIG. 4. The Fourier back-filtered first- and second-shell DAFS and XAFS signals for a single data set. The symbols are as follows: circles, Cu(111) DAFS; triangles, Cu(222) DAFS; and lines, Cu XAFS. The Cu(111) first- and second-shell DAFS signals have been shifted by 90° and the Cu(222) first- and second-shell DAFS signals have been shifted by 67° .

ing the XAFS ratio method to calculate the relative distance shift between each DAFS signal treated as an "unknown" and the Cu XAFS signal treated as a "known" standard, yields Cu(111) first shell ± 0.005 Å and second shell ± 0.015 Å; Cu(222) first shell ± 0.015 Å and second shell ± 0.015 Å. This demonstrates that DAFS measurements can be used to provide neighbor distances with accuracies comparable to XAFS measurements and that experimental, or theoretical, XAFS standards can be used to analyze DAFS measurements by shifting the phases.

The data and analysis presented above demonstrate that for kinematically scattering monatomic systems the measured DAFS intensities contain the same local atomic structural information that is usually obtained by XAFS measurements, and that this local information can be determined easily and precisely from high precision diffraction intensity measurements. However, the potential utility of DAFS as an adjunct and extension of XAFS becomes much clearer when more complex polyatomic and/or spatially structured systems are considered. For these systems, DAFS provides: (1) Spatial selectivity whenever different spatial regions or components of the sample produce diffraction peaks at separate locations in reciprocal space. Then the local atomic structure of each region or component can be measured using one of its characteristic diffraction peaks. Examples include mixed phase powders, strained or compositionally modulated single layers or multilayers, and surface and buried monolayers or reconstructed layers. (2) Site selectivity whenever the inequivalent sites have different diffraction structure factor contributions. Then the DAFS signals for different Bragg peaks can be combined to determine the individual inequivalent site DAFS contributions and the associated local atomic structure.

In favorable cases, some reflections will be dominated by a single site and the separation is easy; in general, the separation is analogous to x-ray crystallography except the linear contributions now contain both the usual x-ray structure factors and the DAFS χ factors. Preliminary demonstrations of both sensitivities have been obtained: spatial selectivity by separating inequivalent InGaAs layers on a GaAs substrate and site selectivity by separating the inequivalent copper sites in 123 superconductor films [8].

-
- [1] P. A. M. Dirac, Proc. R. Soc. London A **114**, 243 (1927); **114**, 710 (1927).
 - [2] G. Wendin, Phys. Scr. **21**, 535 (1979).
 - [3] For example, Y. Cauchois and C. Bonnelle, C.R. Acad. Sci. **242**, 1596 (1956); S. I. Salem and V. L. Hall, J. Phys. F **10**, 1967 (1980); D. H. Templeton *et al.*, Acta Crystallogr. A **36**, 436 (1980).
 - [4] I. Arcon, A. Kodre, D. Glavic, and M. Hribar, J. Phys. (Paris), Colloq. **48**, C9-1105 (1987).
 - [5] See, for example, L. Gerward, G. Thuesen, M. S. Jensen, and I. Alstrup, Acta Crystallogr. A **35**, 852 (1979); M. Blume, J. Appl. Phys. **57**, 3615 (1985), and references therein.
 - [6] For a review and references, see D. H. Templeton, in *Handbook on Synchrotron Radiation*, edited by G. Brown and D. E. Moncton (Elsevier, Amsterdam, 1991), Vol. 3.
 - [7] H. K. Wagenfeld, Z. Phys. B **65**, 437 (1987).
 - [8] H. Stragier, J. O. Cross, J. J. Rehr, Larry B. Sorensen, C. E. Bouldin, and J. C. Woicik (to be published).
 - [9] See, for example, *X-Ray Absorption: Principles, Applications, Techniques of EXAFS, SEXAFS, and XANES*, edited by R. Prins and D. Koningsberger (Wiley, New York, 1988).